INTERNATIONAL JOURNAL FOR NUMERICAL METHODS IN FLUIDS
Int. J. Numer. Meth. Fluids 2008; **57**:1349–1370
Published online 14 April 2008 in Wiley InterScience (www.interscience.wiley.com). DOI: 10.1002/fld.1744

First- and second-order sensitivity equation methods for value and shape parameters

F. Ilinca[1,*,†], D. Pelletier[2] and A. Hay[3]

[1]*National Research Council, 75 de Mortagne, Boucherville, Que., Canada J4B 6Y4*
[2]*École Polytechnique de Montréal, Montréal, Que., Canada H3C 3A7*
[3]*Virginia Tech, Blacksburg, VI 24061-0531, U.S.A.*

SUMMARY

This paper presents formulations of the sensitivity equation method (SEM) and applications to transient flow problems. Solutions are shown for both *value* and *shape* parameters using a three-dimensional solution algorithm. Sensitivities are used for fast evaluation of the flow at nearby values of the parameters: the solution is approximated by a Taylor series in parameter space involving the flow sensitivities. The accuracy of nearby flows is much improved when second-order sensitivities are used. We show how the sensitivity of the Strouhal number can be obtained from the flow sensitivities. Results are in agreement with the experimental correlation. The methodology is also applied to the flow past a cylinder in ground proximity. The proposed method is verified on a steady-state problem by comparing the computed sensitivity with the actual change in the solution when a small perturbation is imposed on the shape parameter. We then investigate the ability of the SEM to anticipate the unsteady flow response to changes in the ground to cylinder gap. The approach properly reproduces the damping or amplification of the vortex shedding with a reduction or increase of the gap size.

Received 20 September 2007; Revised 4 December 2007; Accepted 7 December 2007

KEY WORDS: sensitivity equations; three-dimensional finite elements; time-dependent flows; second-order sensitivity; shape sensitivity; incompressible flows

1. INTRODUCTION

Flow sensitivities are essentially the derivatives of dependent flow variables (velocity, pressure, temperature) with respect to parameters of interest. These fall under two categories. *Value* param-

*Correspondence to: F. Ilinca, National Research Council, Industrial Materials Institute, 75 de Mortagne, Boucherville, Qué., Canada J4B 6Y4.
†E-mail: florin.ilinca@cnrc-nrc.gc.ca

Contract/grant sponsor: NSERC
Contract/grant sponsor: Canada Research Chair Program

eters do not affect the geometry of the computational domain and lend themselves to a simple numerical treatment; for example, an inflow velocity or a coefficient in a constitutive equation. *Shape* parameters are more challenging because a variation of their values causes changes to the geometry of the computational domain; examples include coefficients in a Bezier curve, or coordinates and weights of control points in a NURBS.

The word *sensitivities* has two different meanings. In design optimization it represents the gradient of the cost function [1, 2], whereas in fluid mechanics it refers to the derivatives of the flow solution (velocity, pressure, temperature, etc.) with respect to the parameters of interest. Consider, for instance, the flow around an airfoil at an angle of attack α. Then $\partial\mathbf{u}/\partial\alpha$, $\partial p/\partial\alpha$ are the velocity and pressure flow sensitivities with respect to the airfoil angle of attack. It expresses how the flow field responds to perturbations of α around its nominal value. For the latter, it is therefore probably better to use the term *flow sensitivities*. In both cases, however, sensitivities measure the importance of changes in the response (cost function or flow) to perturbations of the design or model parameters.

Note that flow sensitivities have an intrinsic meaning that does not depend on the existence or statement of an optimal design problem. If, however, one is interested in finding α that minimizes $J(\mathbf{u}(\alpha), p(\alpha), \alpha)$ (say, for example, the drag to lift ratio of an airfoil) then the gradient of J with respect to α may be obtained by adjoint methods or by the implicit differentiation of the objective function

$$\frac{\mathrm{d}}{\mathrm{d}\alpha}J(\mathbf{u}(\alpha), p(\alpha), \alpha) = \frac{\partial J}{\partial \mathbf{u}}\frac{\partial \mathbf{u}}{\partial \alpha} + \frac{\partial J}{\partial p}\frac{\partial p}{\partial \alpha} + \frac{\partial J}{\partial \alpha} \tag{1}$$

where the terms $\partial\mathbf{u}/\partial\alpha$ and $\partial p/\partial\alpha$ are the flow sensitivities.

In design optimization, adjoint formulations are often the preferred route because only one adjoint problem needs to be solved independently of the number of design variables. By contrast, in the sensitivity equation method (SEM) one sensitivity system must be solved for each design parameter. We note, however, that when several cost functions are to be considered, say as in multi-point objective or multi-objective optimization, one must construct and compute as many adjoint solutions as there are objective functions. In this case, flow sensitivities need only to be computed once! Thus, the advantage of an adjoint formulation is not as clear. Moreover, flow sensitivities can be used for other non-optimization purposes. A first use is characterizing the relative importance of parameters (i.e. where and when does parameter a play a key role in determining the flow response). A second use is in ranking parameters in order of importance to reduce the size of the design space. It can also serve to cascade input data uncertainties through a computational fluid dynamics (CFD) code to provide estimates of the uncertainty of the flow response (as in robust design) or to determine the accuracy needed on input data to ensure a level of accuracy in the flow response. Flow sensitivities are also a very efficient approach for fast evaluation of flows at nearby values of the parameters. Efficiency arises from the fact that sensitivities can be obtained at a fraction of the cost of a flow solve and then used in a Taylor series expansion in parameter space around a baseline solution without resulting in a full re-analysis at the perturbed value of the parameter. For time-dependent flows, sensitivities appear to be able to foretell changes in the flow structure long before they can be detected by looking at the flow time signals, thus offering excellent possibilities in flow control [3].

Sensitivity analysis is a more advanced field in solid mechanics than in fluid dynamics. Indeed, textbooks have been written on sensitivity analysis of structures [4, 5]. To our knowledge there is only one book on sensitivity analysis of flow problems [6]. It is recent and more specialized than

DOI: 10.1002/fld

structural mechanics books. Gunzburger [7] discusses sensitivity analysis in the context of flow control and optimization.

There are several means of computing flow sensitivities: finite differences (FDs) of flow solutions, the complex step method [8, 9], automatic differentiation [10], and SEMs [6, 11, 12]. The FD approach is a well-known technique of estimating derivatives. It is based on the following approximation of the derivative of a function f:

$$\frac{\mathrm{d}f}{\mathrm{d}x} \approx \frac{f(x+h)-f(x)}{h} \tag{2}$$

The truncation error is $\mathcal{O}(h)$, and thus this is a first-order approximation of the derivative. Note that in our case, a full Navier–Stokes simulation must be performed for each evaluation of f. Higher-order FD stencils can be derived, at the cost of additional flow evaluations. This option is thus costly because the problem must be solved for two or more values of each parameter of interest. For example, if $\mathbf{a}$ represents a vector of 10 parameters with respect to which we need to compute the flow sensitivity, then 11 flow evaluations are required; one for the baseline values of $\mathbf{a}_0$, and one per perturbation for each of the 10 parameters. In the case of a shape parameter, further technical problems arise because non-matching meshes are obtained for different values of the shape parameter.

The complex-step method as a computational tool for evaluating derivatives was demonstrated by Lyness and Moler [13]. It requires a complete rewrite of the software in complex variables. While this can be automated, it has a significant impact on performance.

Automatic differentiation (also known as algorithmic differentiation or computational differentiation) is a well-established method for estimating derivatives. The method is based on the application of the chain rule of differentiation to each operation in the program simulating the flow. It is equivalent to differentiating the discrete equations to generate a system of equations for the discrete sensitivities. It is powerful because it automatically generates the code for calculating sensitivities [14]. In many cases, implementation requires human intervention to ensure efficiency of the code. Automatic differentiation for first-order flow sensitivities is discussed by Sherman *et al.* [15] and Putko *et al.* [10].

Approaches to calculating sensitivities also differ depending on the order of the operations of approximation and differentiation. In the *discrete* sensitivity equation approach, the total derivative of the flow approximation with respect to the parameter is calculated [4], whereas in the *continuous* SEM one differentiates the continuum equations to yield differential equations for the continuous sensitivities [11]. See Kleiber *et al.* [5] for a discussion of the two approaches. We have adopted the latter approach.

Continuous SEMs may be found in Godfrey and Cliff [16, 17], Borggaard and Burns [11], Limache [18], and Turgeon *et al.* [19] for aerodynamics applications. Application to heat conduction is reported by Blackwell *et al.* [20]. Sensitivities for incompressible flows with heat transfer may be found in several references [12, 21, 22]. Sensitivity analysis for turbulence models is detailed in the works by Godfrey and Cliff [17] and Turgeon *et al.* [23]. Solution of the sensitivity equations for the transient incompressible flow of non-Newtonian fluids is presented by Ilinca *et al.* [24]. A wide variety of flow regimes were treated by the authors [12, 21–23]. This body of work has shown that sensitivities provide an enriched basis of information on which to develop an understanding of complex flow problems. The method was further extended to transient laminar flow by Hristova *et al.* [25], and Ilinca *et al.* [26] and to shape parameters of unsteady flows by Ilinca *et al.* [3] and Ilinca and Pelletier [27].

DOI: 10.1002/fld

This paper presents a formulation of the SEM valid for *value* and *shape* parameters and applicated to steady and unsteady laminar flows. For the case of value parameters a general formulation of the SEM is given for second-order sensitivities. The paper is organized as follows. First, we present the equations describing time-dependent laminar flow along with their boundary and initial conditions. The first- and second-order sensitivity equations and their boundary/initial conditions are then described. The approach is first applied to the flow around a circular cylinder and sensitivities are used to compute nearby flows. Emphasis is put on the *St–Re* relationship and the computed sensitivity of the Strouhal number. The methodology is then applied to the flow past a cylinder in ground proximity. The study investigates the ability of the SEM to anticipate the unsteady flow response to changes in the ground to cylinder gap. The paper ends with conclusions.

2. FLOW EQUATIONS

The flow regime of interest is modeled by the momentum and continuity equations:

$$\rho\frac{\partial \mathbf{u}}{\partial t}+\rho\mathbf{u}\cdot\nabla\mathbf{u}=-\nabla p+\mathbf{f}+\nabla\cdot[2\mu\boldsymbol{\gamma}(\mathbf{u})] \tag{3}$$

$$\nabla\cdot\mathbf{u}=0 \tag{4}$$

where ρ is the density, $\mathbf{u}$ is the velocity, p is the pressure, μ is the viscosity, t represents time, $\boldsymbol{\gamma}(\mathbf{u})=(\nabla\mathbf{u}+\nabla\mathbf{u}^{\mathrm{T}})/2$ is the shear rate tensor, and $\mathbf{f}$ is a body force. The above system is closed with a proper set of initial conditions

$$\mathbf{u}(\mathbf{x},t=0)=\mathbf{u}_0(\mathbf{x}) \quad \text{in } \Omega \tag{5}$$

and Dirichlet and Neumann boundary conditions

$$\mathbf{u}(\mathbf{x},t)=\mathbf{u}_{\mathrm{D}}(\mathbf{x},t) \quad \text{on } \Gamma_{\mathrm{D}} \tag{6}$$

$$\mathbf{t}=[-p\mathbb{I}+2\mu\boldsymbol{\gamma}(\mathbf{u})]\cdot\hat{\mathbf{n}}=\mathbf{F}^{\mathrm{N}} \quad \text{on } \Gamma_{\mathrm{N}} \tag{7}$$

where $\mathbf{u}_{\mathrm{D}}$ is the value of the velocity imposed along the boundary Γ_{D}, $\mathbb{I}$ is the identity tensor, and $\mathbf{F}^{\mathrm{N}}$ is the imposed boundary distribution of the surface traction force $\mathbf{t}$.

The flow equations are solved by a finite element method on three-dimensional meshes. Velocity and pressure are discretized using equal-order interpolations (P1-P1 tetrahedral elements) and equations are solved by a streamline-upwind Petrov Galerkin (SUPG) finite element method [26].

3. SENSITIVITY EQUATIONS

3.1. General formulation of first-order sensitivity equations

The continuous sensitivity equations (CSEs) are derived formally by implicit differentiation of the flow equations (3) and (4) with respect to parameter a. We treat the flow variable $\mathbf{u}$ and p as functions of space, time and of the parameter a. This dependence is denoted as $\mathbf{u}(\mathbf{x},t;a)$ and $p(\mathbf{x},t;a)$. The velocity and pressure sensitivities are defined as the partial derivatives $\mathbf{s}_u^a=\partial\mathbf{u}/\partial a$ and $s_p^a=\partial p/\partial a$, whereas the derivatives of the fluid properties and other flow parameters are

DOI: 10.1002/fld

denoted by a ($'$) and the subscript a (as example $\mu'_a = \mathrm{d}\mu/\mathrm{d}a$ for the sensitivity of the viscosity). Differentiation of Equations (3) and (4) yields

$$\rho'_a\left(\frac{\partial \mathbf{u}}{\partial t}+\mathbf{u}\cdot\nabla\mathbf{u}\right)+\rho\left(\frac{\partial \mathbf{s}_u^a}{\partial t}+\mathbf{u}\cdot\nabla\mathbf{s}_u^a+\mathbf{s}_u^a\cdot\nabla\mathbf{u}\right)=-\nabla s_p^a+\mathbf{f}'_a+\nabla\cdot[2\mu'_a\boldsymbol{\gamma}(\mathbf{u})+2\mu\boldsymbol{\gamma}(\mathbf{s}_u^a)] \tag{8}$$

$$\nabla\cdot\mathbf{s}_u^a=0 \tag{9}$$

3.2. General formulation of second-order sensitivity equations

The same approach is applied to obtain second-order sensitivity equations. Here, we consider two independent parameters a and b. Thus, $\mathbf{u}$ can be expressed as $\mathbf{u}(\mathbf{x}, t; a, b)$. Second-order flow sensitivities are defined as the partial derivatives $\mathbf{s}_u^{ab}=\partial^2\mathbf{u}/\partial a\partial b$ and $s_p^{ab}=\partial^2 p/\partial a\partial b$, and denoting the second-order derivatives of the fluid properties and other flow parameters by a ($''$) and the subscript ab, differentiation of Equations (3) and (4) yields

$$\begin{aligned}&\rho''_{ab}\left(\frac{\partial \mathbf{u}}{\partial t}+\mathbf{u}\cdot\nabla\mathbf{u}\right)+\rho'_a\left(\frac{\partial \mathbf{s}_u^b}{\partial t}+\mathbf{u}\cdot\nabla\mathbf{s}_u^b+\mathbf{s}_u^b\cdot\nabla\mathbf{u}\right)+\rho'_b\left(\frac{\partial \mathbf{s}_u^a}{\partial t}+\mathbf{u}\cdot\nabla\mathbf{s}_u^a+\mathbf{s}_u^a\cdot\nabla\mathbf{u}\right)\\&+\rho\left(\frac{\partial \mathbf{s}_u^{ab}}{\partial t}+\mathbf{u}\cdot\nabla\mathbf{s}_u^{ab}+\mathbf{s}_u^b\cdot\nabla\mathbf{s}_u^a+\mathbf{s}_u^a\cdot\nabla\mathbf{s}_u^b+\mathbf{s}_u^{ab}\cdot\nabla\mathbf{u}\right)\\&=-\nabla s_p^{ab}+\mathbf{f}''_{ab}+\nabla\cdot[2\mu''_{ab}\boldsymbol{\gamma}(\mathbf{u})+2\mu'_b\boldsymbol{\gamma}(\mathbf{s}_u^a)+2\mu'_a\boldsymbol{\gamma}(\mathbf{s}_u^b)+2\mu\boldsymbol{\gamma}(\mathbf{s}_u^{ab})]\end{aligned} \tag{10}$$

$$\nabla\cdot\mathbf{s}_u^{ab}=0 \tag{11}$$

3.3. Initial and boundary conditions

Initial conditions for the sensitivity equations are obtained by implicit differentiation of Equation (5)

$$\mathbf{s}_{\mathbf{u}}^a(\mathbf{x}, t=0)=\frac{\partial \mathbf{u}_0}{\partial a}(\mathbf{x}) \quad \text{in } \Omega \tag{12}$$

$$\mathbf{s}_{\mathbf{u}}^{ab}(\mathbf{x}, t=0)=\frac{\partial^2 \mathbf{u}_0}{\partial a\partial b}(\mathbf{x}) \quad \text{in } \Omega \tag{13}$$

Dirichlet and Neumann boundary conditions are obtained in a similar manner. However, if a is a shape parameter, the position of the boundary is also parameter dependent. Therefore, the differentiation must account for the dependence on a of both the boundary data and the boundary location. For Dirichlet boundary conditions we require that the material derivative of the flow velocity be equal to that of $\mathbf{U}_\mathrm{D}$:

$$\frac{\mathrm{D}\mathbf{u}}{\mathrm{D}a}=\frac{\mathrm{D}\mathbf{U}_\mathrm{D}}{\mathrm{D}a} \quad \text{on } \Gamma_\mathrm{D} \tag{14}$$

$$\frac{\partial \mathbf{u}}{\partial a}+\nabla\mathbf{u}\cdot\frac{\partial \mathbf{x}}{\partial a}=\frac{\partial \mathbf{U}_\mathrm{D}}{\partial a} \quad \text{on } \Gamma_\mathrm{D} \tag{15}$$

DOI: 10.1002/fld

thus we obtain

$$\mathbf{s}_{\mathbf{u}}^{a} = \frac{\partial \mathbf{U}_{\mathrm{D}}}{\partial a} - \nabla \mathbf{u} \cdot \frac{\partial \mathbf{x}}{\partial a} \quad \text{on } \Gamma_{\mathrm{D}} \tag{16}$$

Similar reasoning leads to the following Neumann condition:

$$\begin{aligned} &[-s_p^a \mathbf{I} + 2(\mu \boldsymbol{\gamma}(\mathbf{s}_{\mathbf{u}}^{a}) + \mu_a' \boldsymbol{\gamma}(\mathbf{u}))] \cdot \hat{\mathbf{n}} \\ &= \frac{\partial \mathbf{F}^{\mathrm{N}}}{\partial a} - \left\{ \nabla \cdot [-p\mathbf{I} + 2\mu \boldsymbol{\gamma}(\mathbf{u})] \cdot \frac{\partial \mathbf{x}}{\partial a} \right\} \cdot \hat{\mathbf{n}} - [-p\mathbf{I} + 2\mu \boldsymbol{\gamma}(\mathbf{u})] \cdot \frac{\partial \hat{\mathbf{n}}}{\partial a} \quad \text{on } \Gamma_{\mathrm{N}} \end{aligned} \tag{17}$$

Equation (16) shows that the flow gradients at the wall are needed to evaluate Dirichlet boundary conditions for the sensitivities. Equation (17) reveals that second-order derivatives of velocity are needed in the case of a Neumann boundary condition for a shape parameter. Even higher-order derivatives would be needed if second-order sensitivities were to be computed with respect to a shape parameter. However, in this work we only consider Dirichlet boundary conditions for first-order sensitivities with respect to shape parameters. The dependence of the sensitivities boundary conditions on the flow gradient introduces numerical difficulties when solving CSE, since approximate gradients are used. Sensitivity boundary conditions are evaluated by extracting the normal derivatives from local finite element problems on patches of elements surrounding the boundary nodes [27].

3.4. Finite element solution

There are many choices possible for solving the flow and sensitivity equations. In theory, one can solve the CSE by any numerical method [16, 17]. In practice, it is convenient and cost-effective to use the same finite element method for the flow and the CSE. Indeed, note that the CSE amount to a Newton linearization of the Navier–Stokes equations. Thus, if one uses Newton's method for solving the finite element equations for the flow, the flow sensitivity equations will have the same finite element matrix. Only the right-hand side will differ. This results in substantial savings since the matrix of the first- and second-order sensitivities need not be recomputed or factored if direct solvers are used. In the case of iterative solvers one may reuse the matrix and its preconditioner from the Newton solution to solve the CSE. In practice, the solution for the sensitivity with respect to one parameter is obtained at approximately 10–20% of the cost of solving the flow equations. In this work, sensitivity equations are discretized using the same SUPG finite element formulation as for the flow equations.

4. IMPLEMENTATION

The flow and sensitivity equations are solved on three-dimensional meshes. Time is discretized by an implicit Euler scheme and the equations are linearized with Newton's method. The solution algorithm works as follows:

At each time step

- iterate over the non-linear Navier–Stokes equations (3) and (4) until convergence. A few steps of successive substitution (Picard's method) are performed at the beginning of the first time step and the Newton's linearization is used afterward;

DOI: 10.1002/fld

- for *shape* parameters: evaluate the solution gradient at the boundary and impose boundary conditions for the sensitivity equations;
- use the matrix from the last Newton iteration on the flow problem and solve the linear system for the sensitivity equations (8) and (9). This step requires the evaluation of one right-hand side and one linear equation solve per parameter;
- use the same approach for the second-order sensitivities. Again this requires one right-hand side evaluation and one matrix solve per second-order sensitivity.

Element matrices are constructed using a numerical Jacobian technique and assembled in a compressed sparse row format. Flow and sensitivity global systems are solved by BiCG preconditioned iterative methods.

We have used strict tolerances in order to control computational errors that may arise due to several factors. The most important one is iterative convergence of the non-linear iterations by Newton's method and the convergence criteria for stopping the iterative solution of the linearized system within a Newton iteration. Numerical tests were carried out to assess the influence of these criteria and revealed that Newton tolerances of 10^{-6} in relative values for both the equation residual and the correction of the solution were sufficient to guarantee accurate numerical solutions. Similarly, stopping the BiCG solver when residuals drop by 6 orders of magnitude proved sufficient.

5. NUMERICAL RESULTS

In our previous work [26], the numerical approach was verified using the method of manufactured solutions [28]. In such a case, the direct differentiation of the manufactured solution provides closed-form expressions for the sensitivities. The grid and time-step refinement study showed that the flow and sensitivity solutions are accurate and the algorithm recovers the theoretical grid convergence rate. The sensitivity solution can also be verified by estimating the flow gradients with respect to a using FDs [3, 26]. For this, the design parameter a is changed by a small amount δa and the solution is recomputed. The reference FD flow sensitivities are determined from

$$\left(\frac{\partial \mathbf{u}}{\partial a}\right)_{\mathrm{FD}} = \frac{\mathbf{u}(a+\delta a)-\mathbf{u}(a-\delta a)}{2\delta a} + \mathcal{O}(\delta a^2) \tag{18}$$

$$\left(\frac{\partial^2 \mathbf{u}}{\partial a^2}\right)_{\mathrm{FD}} = \frac{\mathbf{u}(a+\delta a)-2\mathbf{u}(a)+\mathbf{u}(a-\delta a)}{\delta a^2} + \mathcal{O}(\delta a^2) \tag{19}$$

in which δa is taken very small compared with a ($10^{-2}a$ to $10^{-4}a$). The FD gradients should be used with care for transient flows with unbounded time evolution of the solution sensitivity. The error in the FDs gradient depends on the magnitude of high-order derivatives, which increase at a faster rate than the solution and its first-order derivative. Hence, the FD sensitivity is reliable only in the first few instants of the simulation, when higher-order terms are negligible [26].

In this section, we present various transient laminar flow applications on which the sensitivity of the flow is computed with respect to value and shape parameters.

DOI: 10.1002/fld

5.1. *Uniform flow around a circular cylinder*

5.1.1. Problem statement. The computational domain and boundary conditions for this problem are shown in Figure 1(a). Because the problem is two-dimensional, only a slab was meshed with three-dimensional tetrahedral elements. The mesh is shown in Figure 1(b) and was designed to provide adequate refinement in the boundary layer where gradients are higher and in the wake of the cylinder where the solution is expected to exhibit larger time variations. A steady velocity profile was imposed at the inflow. The first computations were carried out for a Reynolds number $Re=\rho U_0 d/\mu$ equal to 100, for which a vortex street forms in the wake of the cylinder. Because the computational domain and mesh are symmetrical, the vortex street is determined by truncation errors and non-linear iterative convergence parameters which are difficult to characterize and use as model parameters. To provide a rigorously controlled framework to investigate the vortex street sensitivities we use a perturbation of the uniform velocity profile as a trigger mechanism for vortex formation. The inflow velocity is given by

$$U_f = U_0(1+U_p g(y)) \tag{20}$$

where $U_0=1$ is the value of the free-stream velocity, U_p is a small velocity perturbation set to 10^{-3} and $g(y)$ is an anti-symmetric function taking values between -1 and 1. Here we have used the form

$$g(y)=\tanh(\beta y) \tag{21}$$

with $\beta=10$. This approach ensures that small changes in parameter values will induce small changes in the behavior of the flow.

The initial conditions are obtained from a steady-state solution of the flow and sensitivity equations. Following the work of Sohankar *et al.* [29] the time step is set to $\Delta t=0.025$. This leads to about 240 time steps per period of vortex shedding. Sensitivities are computed with respect to the inlet velocity U_0. The only non-zero boundary condition for the sensitivities are those at the inlet. Flow variables may either be seen as dimensionless or as having consistent dimensions such as the length measured in m, the velocity in m/s and the time in s. Here we use the free-stream velocity U_0 and the cylinder diameter d as reference quantities.

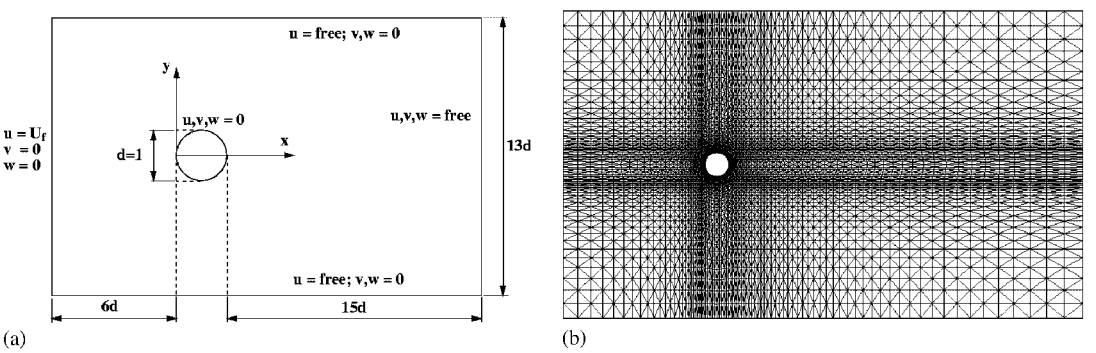

Figure 1. Uniform flow around a circular cylinder: definition and mesh: (a) domain and boundary conditions and (b) mesh.

DOI: 10.1002/fld

5.1.2. Flow response. The initial solution of the transient problem is symmetrical (see the vorticity contours on Figure 2). Figure 3 shows the time variation of the flow velocity at a point located on the symmetry axis one diameter downstream of the cylinder. The signal is shown from time $t=0$ to 160. Note that during the first part of the simulation the transverse velocity v is zero, confirming that the flow is symmetric with respect to the x-axis. The axial velocity u is also constant until approximately $t=60$, after which time perturbations are observed and the solution is no longer symmetrical. The amplitude of these perturbations increases in time and leads to the formation of the well-known Karman vortex street. Because the Reynolds number $Re=100$ is higher than the critical Reynolds number $Re_{cr}=51$ [29], a vortex street develops in the wake of the cylinder. Vorticity contours are shown in Figure 4 from $t=94$ to 100 clearly illustrating the Karman vortex street.

5.1.3. Flow sensitivity responses. The first- and second-order sensitivities represent the slope and curvature of the dependent variables in parameter space. Their time signals at $(x=2, y=0)$ for U_0 as parameter are shown in Figure 5. The following observations can be made:

- the period of the sensitivity signals is the same as the period of the flow;
- sensitivity perturbations from the steady-state solution occur around $t=60$ as was the case for the flow variables;
- time signal of the flow variables exhibit constant amplitude periodic behavior, whereas the sensitivities show an unbounded increase in the signal amplitude;

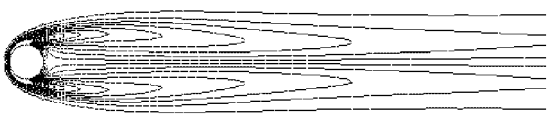

Figure 2. Uniform flow around a circular cylinder: vorticity contours of initial solution.

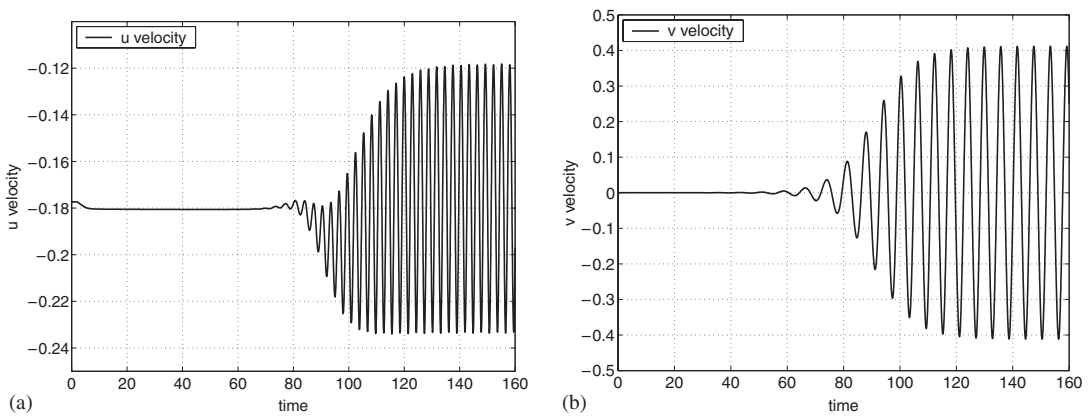

Figure 3. Uniform flow around a circular cylinder: flow response at $(x=2, y=0)$: (a) u-velocity and (b) v-velocity.

DOI: 10.1002/fld

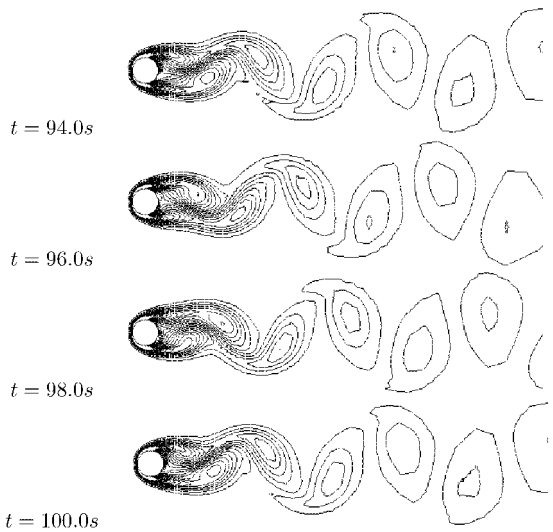

Figure 4. Uniform flow around a circular cylinder: Karman vortex street.

- the amplitude of the sensitivities is much higher than the amplitude of the flow variables. For example, at $t=100$ the v-velocity amplitude has almost reached its maximum value, whereas the amplitude of the first-order sensitivity is about 10^2 times larger and that of the second-order sensitivity is 10^4 times larger and they keep increasing with time.

The continuous sensitivities are verified by comparing them with the FD approximation of the flow gradients with respect to U_0. For this, the inlet velocity U_0 is changed by a small amount δU_0 and the solution is recomputed. The reference FD flow sensitivities are determined from Equations (18) and (19) in which $a=\delta U_0$. As shown in previous work [26], the FD gradient for transient oscillatory flow is very sensitive to the increment δU_0 and can be used as a reference derivative only in the early stage of the flow ($t<80$). Figure 6 compares the continuous sensitivities of the vertical velocity v with FD estimations using $\delta U_0=0.01U_0$ (square symbols) and $\delta U_0=0.001U_0$ (circles), respectively. For the first-order sensitivity the CSE solution compares very well with the FD gradient obtained for $\delta U_0=0.001U_0$. For the second-order sensitivity the agreement is better when comparing with the FD gradient using $\delta U_0=0.01U_0$.

5.1.4. Fast evaluation of nearby flows. Sensitivities can be used for fast evaluation of flows for nearby values of the parameters. The prediction of nearby flows of periodic solutions having an infinite number of derivatives defined is very challenging. Consider, for example, what happens to the v-velocity, when a generic parameter a is subject to a variation δa from its nominal value a_0. The Taylor series expansion reads as

$$v(x, y; a_0+\delta a)=v(x, y; a_0)+\frac{\partial v}{\partial a}\delta a+\frac{\partial^2 v}{\partial a^2}\frac{\delta a^2}{2}+O(\delta a^3) \tag{22}$$

Figure 7 shows the results obtained using first- (square symbols) and second-order (circles) Taylor series for the point $(x=2, y=0)$ and a time interval between $t=60$ and 100. At early

DOI: 10.1002/fld

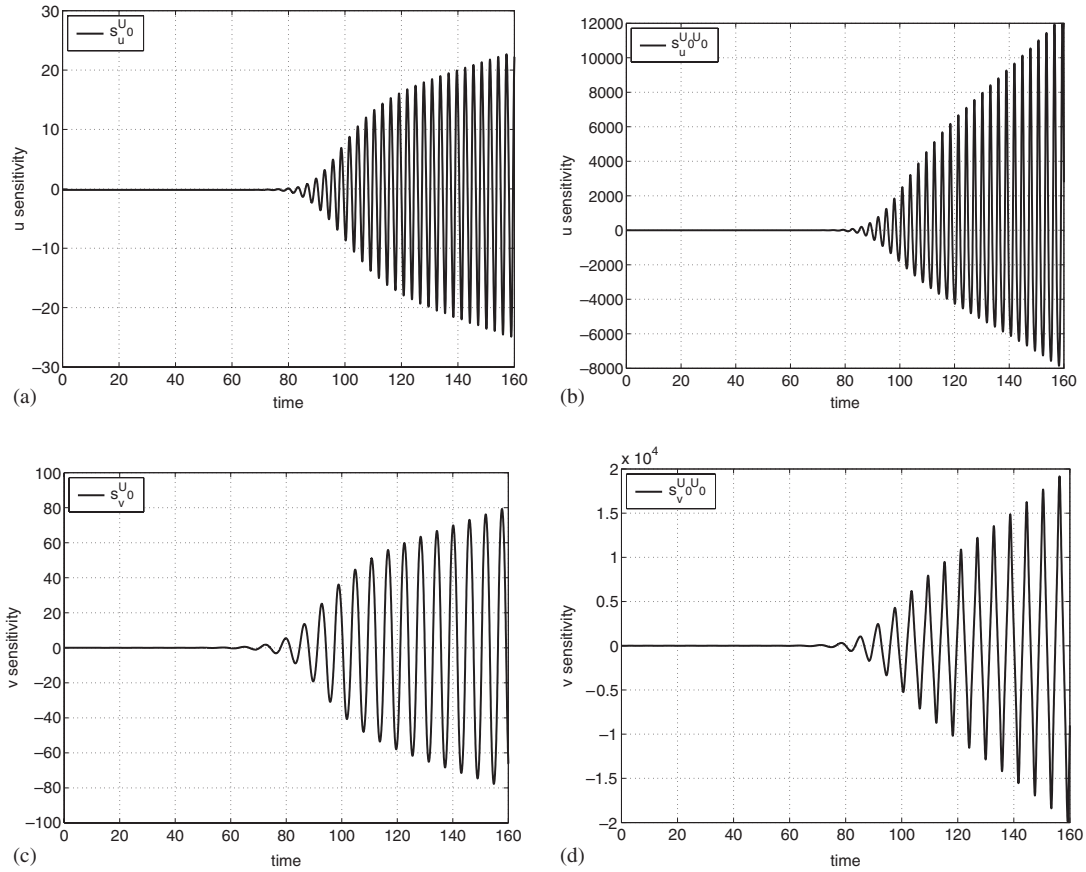

Figure 5. Uniform flow around a circular cylinder: sensitivities with respect to U_0 at $(x=2.0, y=0.0)$: (a) $s_u^{U_0}$; (b) $s_u^{U_0U_0}$; (c) $s_v^{U_0}$; and (d) $s_v^{U_0U_0}$.

times, the two Taylor series approximations of the flow response are in good agreement with the CFD re-analysis at the perturbed value of the parameter $(U_0+\delta U_0)$. As expected given the size of higher-order terms, the agreement deteriorates with time especially at $t>80$. The agreement is better for the vertical velocity v, which exhibits larger amplitude than u. In all cases the second-order Taylor series provides better agreement with the re-analysis than the first-order one. Observe also that the second-order reconstruction is in better phase with the true solution than the first-order reconstruction.

Figure 8 presents the spatial distributions of the v-velocity extrapolations obtained by Taylor series for $\delta U_0=0.01U_0$ compared with those obtained by a full flow reanalysis. Comparisons are shown for a station located at $x=4$, and time ranging from $t=75$ to 80. The baseline solution at the unperturbed value of the parameter is also shown, so that the effect of increasing the order of the Taylor series can be assessed. Results indicate that the accuracy of the extrapolation is much improved when second-order terms are used. In all cases second-order Taylor series extrapolations (open circles) are almost superimposed over the recomputed solution, whereas

DOI: 10.1002/fld

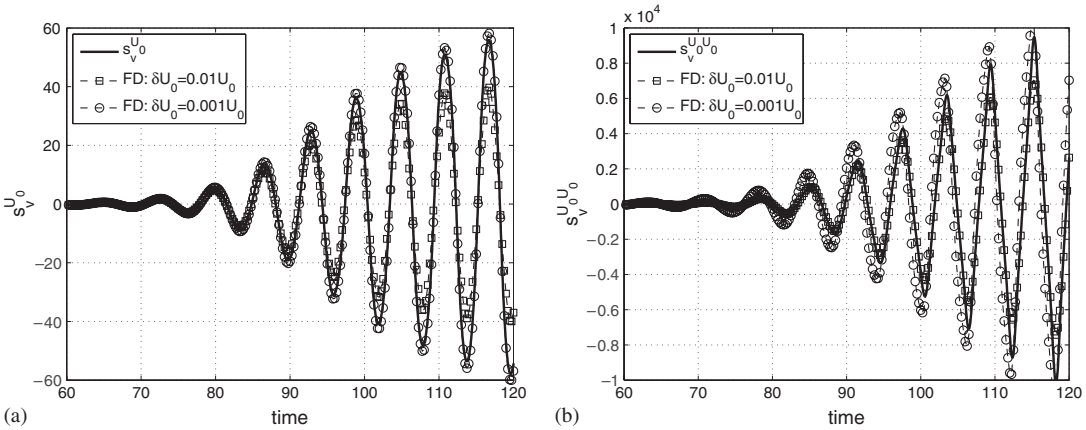

Figure 6. Comparison of CSE and FD sensitivities of v at $(x=2.0, y=0.0)$: (a) $s_v^{U_0}$ and (b) $s_v^{U_0U_0}$.

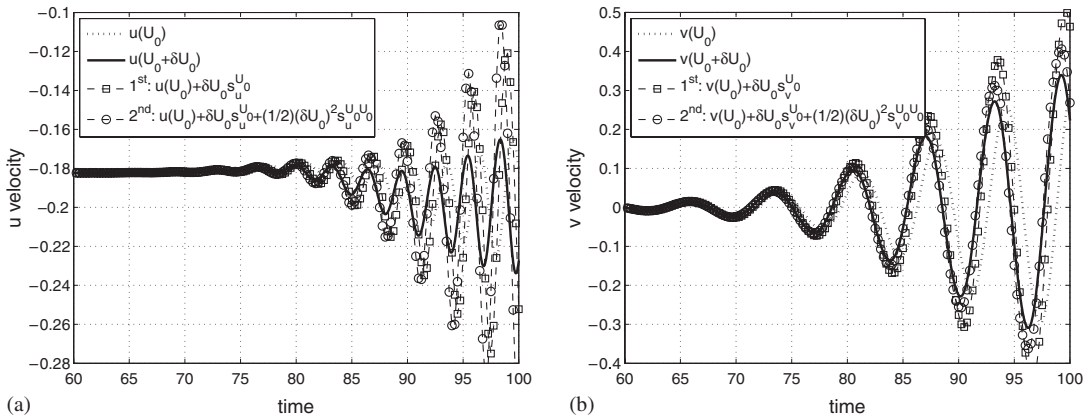

Figure 7. Uniform flow around a circular cylinder: Fast nearby solutions for δU_0 equal to 1% of U_0 at $(x=2.0, y=0.0)$: (a) $u(U_0+\delta U_0)$, $\delta U_0=0.01U_0$ and (b) $v(U_0+\delta U_0)$, $\delta U_0=0.01U_0$.

first-order Taylor extrapolations (square symbols) exhibit higher errors. Observe also that some particular characteristics of the solution, such as the knee in the velocity profile at $y=1$ and $t=78$ (Figure 8(d)) are well captured by the second-order Taylor series, but are entirely missed by first-order approximation.

5.1.5. Sensitivity of the Strouhal number. The Strouhal number St is a standard non-dimensional representation of the vortex-shedding frequency. It is defined as the ratio of the characteristic frequency of the flow response f to the inverse of the fluid dynamics time scale D/U_0, that is the time it takes for a fluid particle moving at velocity U_0 to travel the distance D:

$$St=\frac{f\,D}{U_0} \tag{23}$$

DOI: 10.1002/fld

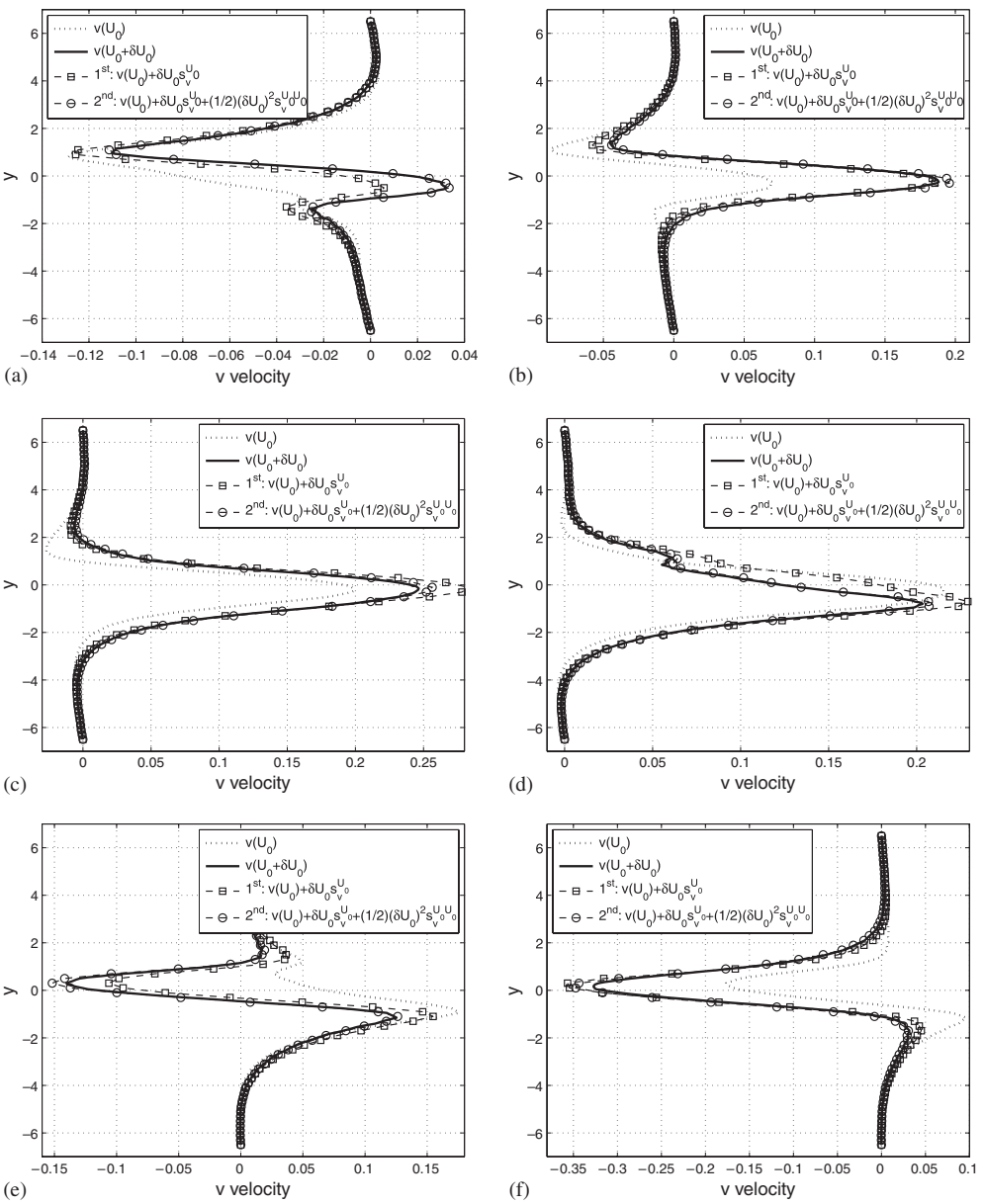

Figure 8. Circular cylinder in uniform flow at $x=4.0$: Extrapolated and true profiles of v for $\delta U_0 = 0.01 U_0$: (a) v component at $t=75$; (b) v component at $t=76$; (c) v component at $t=77$; (d) v component at $t=78$; (e) v component at $t=79$; and (f) v component at $t=80$.

It is well known that the Strouhal number depends on the Reynolds number of the flow. Figure 9(a) compares the predicted Strouhal number to the correlation due to Williamson [30]. Results from a mesh refinement study show that the prediction gets closer to measurements as the mesh is refined

DOI: 10.1002/fld

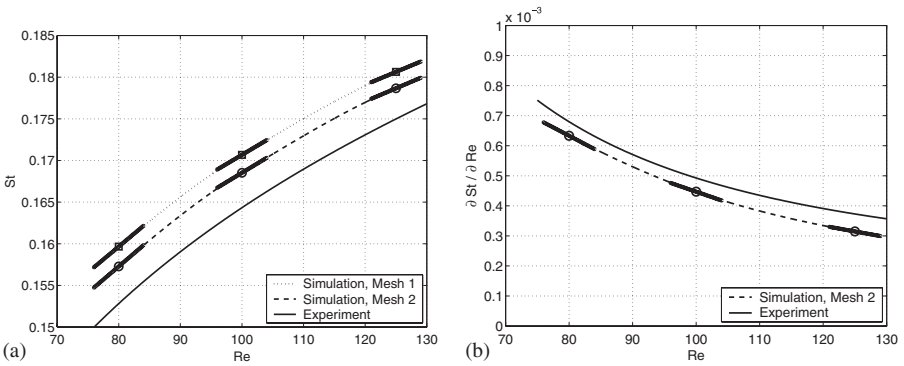

Figure 9. Uniform flow around a circular cylinder: (a) Strouhal dependence upon Reynolds and (b) variation of the slope $\partial St/\partial Re$ with Re.

and when the outer boundaries are placed farther away from the cylinder [31]. Figure 9(a) indicates that the proper behavior is reproduced and that increasing the distance to the outer boundary will improve the agreement (Mesh 2 compared with Mesh 1).

We now turn our attention to the sensitivity of the Strouhal number with respect to the Reynolds number $\partial St/\partial Re$. While there is no direct way of relating $\partial St/\partial Re$ to the flow sensitivities we can, however, use FD approximations to compute the first- and second-order derivatives of St with respect to the Reynolds number Re:

$$\frac{\partial St}{\partial Re} = \lim_{\delta Re \to 0} \frac{St[\mathbf{u}(Re+\delta Re)] - St[\mathbf{u}(Re-\delta Re)]}{2\delta Re} \tag{24}$$

$$\frac{\partial^2 St}{\partial Re^2} = \lim_{\delta Re \to 0} \frac{St[\mathbf{u}(Re+\delta Re)] - 2St[\mathbf{u}(Re)] + St[\mathbf{u}(Re-\delta Re)]}{(\delta Re)^2} \tag{25}$$

In principle, Equations (24) and (25) require three flow solutions: one at Re, one at $(Re+\delta Re)$, and one at $(Re-\delta Re)$. However, if one has access to first- and second-order flow sensitivities $\mathbf{s}_u^{Re} = \partial \mathbf{u}/\partial Re$, $\mathbf{s}_u^{ReRe} = \partial^2 \mathbf{u}/\partial Re^2$ one can use the following approximations:

$$St[\mathbf{u}(Re+\delta Re)] = St[\mathbf{u}(Re) + \mathbf{s}_u^{Re}\delta Re + \tfrac{1}{2}\mathbf{s}_u^{ReRe}(\delta Re)^2] \tag{26}$$

$$St[\mathbf{u}(Re-\delta Re)] = St[\mathbf{u}(Re) - \mathbf{s}_u^{Re}\delta Re + \tfrac{1}{2}\mathbf{s}_u^{ReRe}(\delta Re)^2] \tag{27}$$

The flow sensitivities with respect to the Reynolds number can be related to the flow sensitivities with respect to the free-stream velocity U_0 as

$$\mathbf{s}_u^{Re} = \frac{U_0}{Re}\mathbf{s}_u^{U_0} \tag{28}$$

$$\mathbf{s}_u^{ReRe} = \left(\frac{U_0}{Re}\right)^2 \mathbf{s}_u^{U_0 U_0} \tag{29}$$

In essence, we replace flow solutions at $(Re+\delta Re)$ and $(Re-\delta Re)$ by Taylor series expansion around the baseline flow $\mathbf{u}(Re)$, thus reducing the cost from three flow solves to one flow and

DOI: 10.1002/fld

Table I. Results for the uniform from around a circular cylinder (Mesh 2).

Re		80	100	125
St	Simulation	0.1573	0.1685	0.1786
	Correlation	0.1528	0.1643	0.1750
$\frac{\partial St}{\partial Re}$	Simulation	0.633×10^{-3}	0.446×10^{-3}	0.314×10^{-3}
	Correlation	0.680×10^{-3}	0.493×10^{-3}	0.373×10^{-3}
$\frac{\partial^2 St}{\partial Re^2}$	Simulation	-1.11×10^{-5}	-0.73×10^{-5}	-0.38×10^{-5}
	Correlation	-1.30×10^{-5}	-0.67×10^{-5}	-0.34×10^{-5}

two sensitivity solutions. Assuming that a sensitivity field can be obtained at approximately 10% of the cost of a flow solution we reduce the effort to 1.2 flow solves. The computed values of the Strouhal number and of its first- and second-order derivatives with respect to the Reynolds number are given in Table I for $Re=80, 100$ and 125. The values corresponding to the correlation of Williamson [30] are also shown. As can be seen the agreement is suprisingly good.

Figure 9(a) illustrates the quality of the estimate of the sensitivity $\partial St/\partial Re$, which turns out to be the slope of the *St vs Re* curve. The short thick segments attached to predictions at $Re=80$, 100 and 125 are the slope predicted by Equation (24). The agreement between our estimate of $\partial St/\partial Re$ and the correlation of Williamson is indeed quite good.

The second-order derivative $\partial^2 St/\partial Re^2$ computed from the solution sensitivities is the slope of the $\partial St/\partial Re$ *vs Re* curve (thicker lines in Figure 9(b)). Here again we see that the agreement is good with the experimental observation. Note that the second-order derivative $\partial^2 St/\partial Re^2$ can only be obtained by solving for the second-order sensitivities of the flow.

5.2. *Shape sensitivity for flow around a circular cylinder in ground proximity*

We consider the more complex flow around a circular cylinder in ground proximity and study the effect of the ground to cylinder gap size s. The computational domain and boundary conditions are shown in Figure 10(a). Because the problem is two dimensional a slab was meshed with one layer of tetrahedral elements. The mesh, shown in Figure 10(b) has 236 800 4-node tetrahedral elements and was designed to provide adequate resolution for both the flow and its sensitivity. Recall that when a boundary is relocated by varying the design parameter, as is the case here with the surface of the cylinder, the Dirichlet boundary conditions for the velocity sensitivities depend on the gradient of the flow. Hence, the accuracy of the recovered nodal derivatives plays a very important role. In the present work, velocity derivatives are determined from local finite element problems on patches of elements surrounding the boundary nodes [27]. Good accuracy was obtained for a mesh having the circumference of the cylinder divided into 256 equal length elements. The inflow velocity U_0 is uniform. The initial conditions are obtained from a steady-state solution of the flow and its sensitivities with respect to s. The Reynolds number $Re=\rho U_0 D/\mu$ is set to 100.

5.2.1. Sensitivity analysis for the steady-state solution. When the gap s is small enough the wall has a strong enough stabilizing effect on the flow to make it stationary. For the present conditions a vortex street develops in the wake of the cylinder. However, steady-state solutions could be obtained by neglecting the time-dependent term in the momentum equations. The steady-state CSE solution

DOI: 10.1002/fld

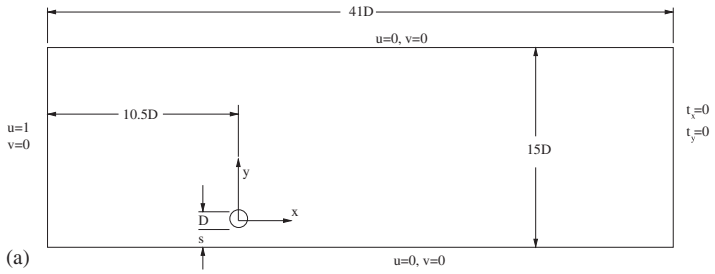

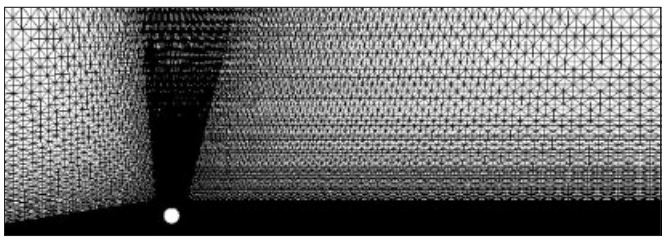

(b)

Figure 10. Flow around a circular cylinder in ground proximity: (a) domain and boundary conditions and (b) mesh.

is verified by computing the flow sensitivities with respect to s by FDs. To this end, the distance to the ground s is changed by a small amount δs and the solution is recomputed. In order to minimize the influence of the mesh changes on the solution, the topology of the mesh is kept the same. Only nodes near the cylinder and found in the box $[-0.75D, 0.75D]\times[-0.75D, 0.75D]$ are displaced when changing s. The accuracy of the sensitivity is then verified at locations outside this subdomain, where the nodes remain at the same location. Here we use points located at $x = D$, one diameter downstream of the center of the cylinder. The reference FD flow sensitivity is determined from

$$\left(\frac{\partial \mathbf{u}}{\partial s}\right)_{\mathrm{FD}} = \frac{\mathbf{u}(s+\delta s)-\mathbf{u}(s-\delta s)}{2\delta s} \tag{30}$$

in which $\delta s = 0.001D$. The accuracy of the solution gradient from Equation (30) is of the order $\mathcal{O}(\delta s^2)$. Figure 11 compares the CSE predictions to FD approximations of s_u and s_v at $x = D$ for steady-state flow and $s = 0.75D$. As can be seen, the two sets of results agree extremely well indicating that the SEM performs well. It also indicates that the flow gradients are computed accurately at the Dirichlet boundary points, as these gradients are used to impose boundary conditions for the sensitivities.

5.2.2. Sensitivity analysis of the unsteady flow. The flow past a cylinder induces steady-state recirculating vortices for small gap values. When the distance to the wall increases above a critical value, vortex shedding is triggered behind the cylinder resulting in the well-known Karman vortex street. We first look at results for the case $s = D$ for which the vortex street develops rapidly. This is clearly seen in Figure 12 which shows vorticity contours for times $t = 104, 106, 108$ and 110 (the time scale is set equal to D/U_0). To quantify the effect of the wall distance on the vortex street formation, simulations were also carried out for a gap size $s = 0.75D$. Vorticity contours are

DOI: 10.1002/fld

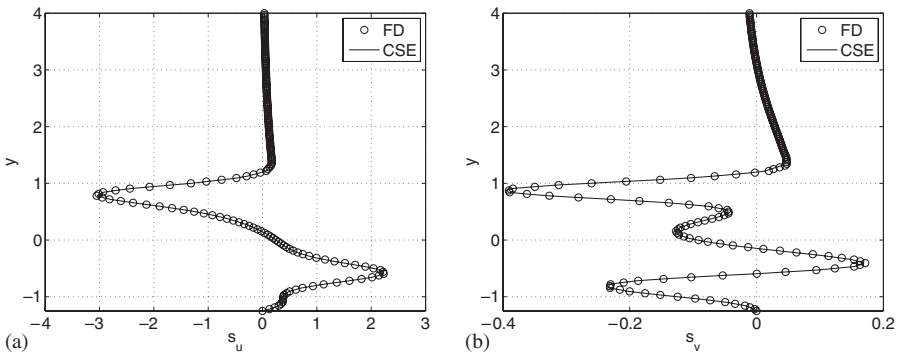

Figure 11. Steady-state flow: verification of the computed sensitivity at $x = D$: (a) s_u and (b) s_v.

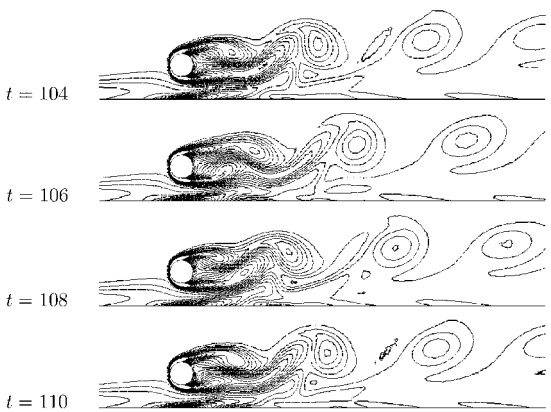

Figure 12. Flow around a circular cylinder at $s = D$ from the wall: Von Karman vortex street.

shown in Figure 13 for $t = 144$ to 150, that is, at latter times than for the case $s = D$ (Figure 12). As can be seen, the vortex street develops more slowly and with smaller amplitudes than for the case $s = D$. This is also seen in Figure 14 which compares the time signal of the vertical velocity v at the point $(x = 4D, y = D)$ for both cases.

Shape sensitivities with respect to the wall distance s were computed for $s = 0.75D$. The time signals at $(x = 4D, y = D)$ for the flow and its sensitivities are shown in Figure 15. The flow solution is shown in the left column of the figure. The SEM sensitivities are compared with a central FD approximation with $\delta s = 0.001D$ (FD in Figure 15). The following observations can be made:

- the periods of the sensitivity signals are the same as those of the flow;
- the amplitudes of the oscillation in sensitivities are larger and increase at a faster rate than those of the flow;
- in all cases the SEM sensitivities agree very well with the FD approximation.

Figure 16 presents the time variations of the oscillation amplitude of the v component of velocity and that of its sensitivity. Both sets of data are plotted on a logarithmic scale. Note that the amplitude

DOI: 10.1002/fld

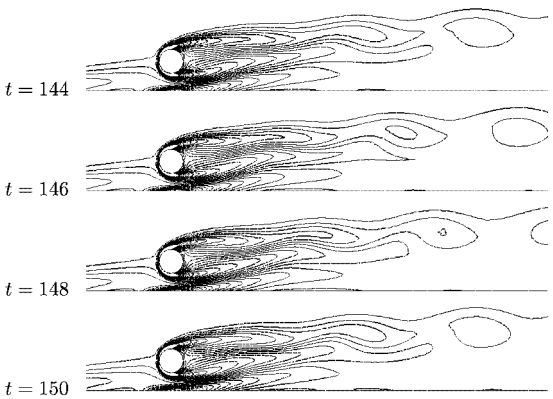

Figure 13. Flow around a circular cylinder at $s = 0.75D$ from the wall: initiation of unstable flow.

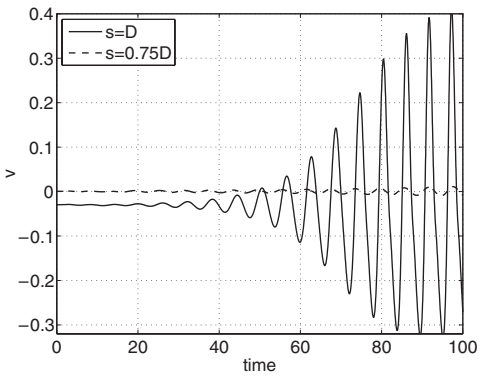

Figure 14. Time signal of the vertical velocity at $(x = 4D, y = D)$.

of the sensitivity signal is much larger and increases faster than that of the flow solution. This is an important observation because it indicates that the sensitivities appear to be reacting faster and more strongly than the flow to changes in the parameter values. In other words, sensitivities appear able to foretell the transition from the steady-state solution to the vortex shedding before it becomes visible in the flow signal. This may prove very useful in flow control applications.

5.2.3. Fast evaluation of flows on nearby geometries. We now show how to use sensitivities for fast evaluation of flows on nearby geometries. Consider, for example, what happens to the u-velocity, when the gap parameter s is subject to a variation δs from its reference value s_0. First-order Taylor series expansion in s yields

$$u(x, y, z, t; s_0 + \delta s) \approx u(x, y, z, t; s_0) + \left.\frac{\partial u}{\partial s}\right|_{s_0} \delta s \tag{31}$$

Using the baseline solution obtained at $s = 0.75D$, we compare the flow estimates from the Taylor series for u and v to a full flow reanalysis at the perturbed values of the parameter, i.e. Equation (31)

DOI: 10.1002/fld

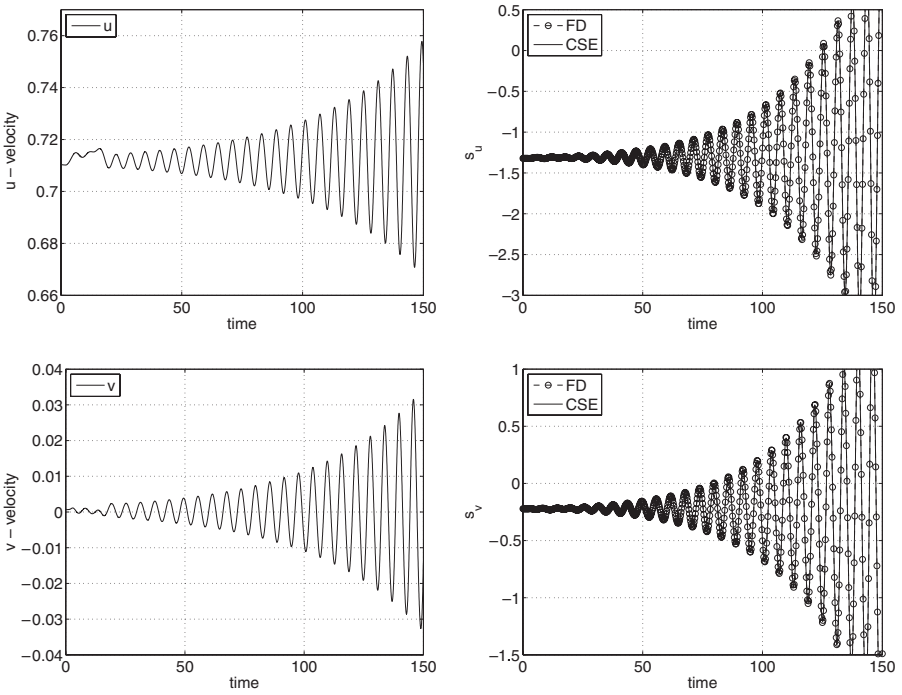

Figure 15. Time signal of the flow and its sensitivities with respect to s at $(x=4D, y=D)$ for $s=0.75D$.

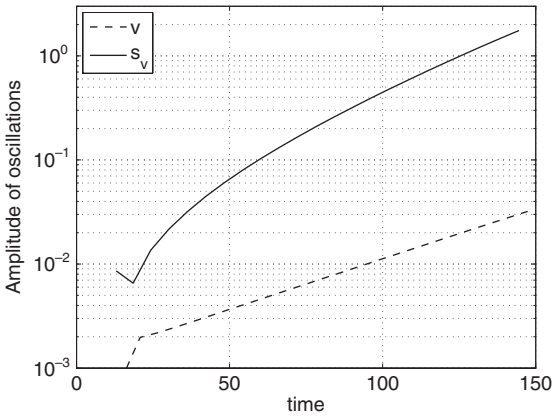

Figure 16. Amplitude of oscillations in v and its sensitivity at $(x=4D, y=D)$ for $s=0.75D$.

vs $u(x, y, z, t; s_0+\delta s)$. Results for $s=0.76D$ are shown in Figure 17 for the point $(x=4D, y=D)$. Note that the location of this point relative to the ground is maintained unchanged when the ground to cylinder gap changes (i.e. the ground is kept fixed and the cylinder is displaced). The reconstructed solutions are very close to those obtained by reanalysis at the perturbed value

DOI: 10.1002/fld

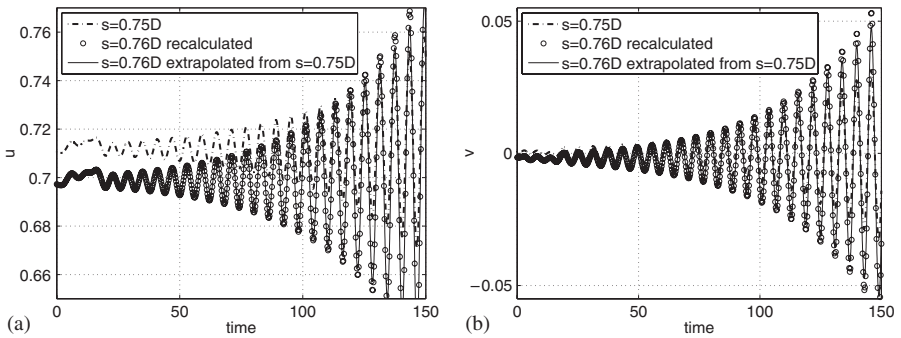

Figure 17. Flow at $(x=4D, y=D)$: fast evaluation of flow at $s=0.76D$ from $s=0.75D$.

of s. The Taylor-series approximations of the flow response are in very good agreement with the CFD reanalysis at early times. Agreement deteriorates very slightly at later times, probably because higher-order derivatives in the Taylor series expansion become important. Observe also that sensitivities provide other quantitative information concerning trends of the flow response. They predict the damping of the vortex shedding when s decreases and the amplification of unsteadiness when the cylinder to ground gap increases.

6. CONCLUSION

A general sensitivity equation formulation was developed for computing first- and second-order sensitivities of time-dependent incompressible laminar flows.

The method was first applied to the flow around a circular cylinder. The flow starts with a symmetrical solution and then goes through a transition phase leading to the usual Karman vortex street characterized by alternate vortex shedding. Taylor series expansions in parameter space using sensitivities were shown to be a powerful tool for fast evaluation of nearby flows. Results indicate that accuracy improves when second-order sensitivities are included in the Taylor series expansions.

Flow sensitivities were used to determine the sensitivity of the Strouhal number with respect to the Reynolds number. The slope of the *St–Re* relationship $\partial St/\partial Re$ and curvature $\partial^2 St/\partial Re^2$ computed using sensitivity information agree well with both the computed and experimental observations of the dependence of *St* on *Re*.

The method was also used to compute shape sensitivities of the flow around a circular cylinder in proximity to the ground. Sensitivities were used to study the influence of the distance to the wall on the amplitude of vortex shedding behind the cylinder. For $s=0.75D$, the amplitudes of the sensitivity oscillations increase much faster with time than those of the flow. Hence, sensitivities provide useful information to anticipate the flow response. Amplification of vortex shedding with increased s/D is well predicted. This property of sensitivities will likely prove useful in developing flow control algorithms to maintain certain characteristics of the flow (for example, minimize the vortex street).

DOI: 10.1002/fld

ACKNOWLEDGEMENTS

This work was sponsored in part by NSERC (Government of Canada) and the Canada Research Chair Program (Government of Canada).

REFERENCES

1. Yang RJ, Choi KK, Haug EJ. Numerical considerations in structural component shape optimization. *Journal of Mechanisms Transmissions and Automation in Design* 1985; **107**(3):334–339.
2. Yang RJ, Choi KK. Accuracy of finite element based shape design sensitivity analysis. *Journal of Structural Mechanics* 1985; **13**(2):223–239.
3. Ilinca F, Hay A, Pelletier D. Shape sensitivity analysis of unsteady laminar flow past a cylinder in ground proximity. *Thirty-sixth AIAA Fluid Dynamics Conference and Exhibit*, San Francisco, CA, June 2006; AIAA Paper 2006-3880.
4. Haug EJ, Choi K, Komkov V. *Design Sensitivity Analysis of Structural Systems*. Mathematics in Science and Engineering, vol. 177. Academic Press: Orlando, 1986.
5. Kleiber M, Antúnez H, Hien TD. *Parametric Sensitivity in Nonlinear Mechanics*. Wiley: New York, 1997.
6. Stanley LG, Stewart DL. *Design Sensitivity Analysis*: *Computational Issues of Sensitivity Equation Methods*. Frontiers in Applied Mathematics, vol. 25. SIAM: Philadelphia, PA, 2001.
7. Gunzburger MD. *Perspectives in Flow Control and Optimization*. SIAM: Philadelphia, PA, 2002.
8. Martins JRRA, Stradza P, Alonso JJ. The complex-step derivative approximation. *ACM Transactions on Mathematical Software—TOMS* 2003; **29**(3):245–262.
9. Lu S-Y, Sagaut P. Direct sensitivity analysis for smooth unsteady compressible flows using complex differentiation design. *International Journal for Numerical Methods in Fluids* 2007; **53**(12):1863–1886.
10. Putko M, Newman P, Taylor A, Green L. Approach for uncertainty propagation and robust design in CFD using sensitivity derivatives. *Fifteenth AIAA Computational Fluid Dynamics Conference*, Anaheim, CA, June 2001; AIAA Paper 2001-2528.
11. Borggaard J, Burns J. A PDE sensitivity equation method for optimal aerodynamic design. *Journal of Computational Physics* 1997; **136**(2):366–384.
12. Turgeon É, Pelletier D, Borggaard J. A general continuous sensitivity equation formulation for complex flows. *Numerical Heat Transfer*, *Part B* 2002; **42**:485–498.
13. Lyness J-N, Moler CB. Numerical differentiation of analytic functions. *SIAM Journal on Numerical Analysis* 1967; **4**(2):202–210.
14. Griewank A. *Evaluating Derivatives*. SIAM: Philadelphia, PA, 2000.
15. Sherman LL, Taylor III AC, Green L, Newman PA, Hou GW, Korivi VM. First- and second-order aerodynamic sensitivity derivatives via automatic differentiation. *Journal of Computational Physics* 1996; **129**(2):307–331.
16. Godfrey AG, Cliff EM. Direct calculation of aerodynamic force derivatives: A sensitivity-equation approach. *Thirty-sixth AIAA Aerospace Sciences Meeting and Exhibit*, Reno, NV, January 1998; AIAA Paper 98-0393.
17. Godfrey AG, Cliff EM. Sensitivity equations for turbulent flows. *Thirty-ninth AIAA Aerospace Sciences Meeting and Exhibit*, Reno, NV, January 2001; AIAA Paper 2001-1060.
18. Limache A. Aerodynamic modeling using computational fluid dynamics and sensitivity equations. *Ph.D. Thesis*, Virginia Polytechnic Institute and State University, Blacksburg, VA, 2000.
19. Turgeon É, Pelletier D, Borggaard J. Computation of airfoil flow derivatives using a continuous sensitivity equation method. *Eighth CASI Aerodynamics Symposium*, Toronto, Canada, April 2001.
20. Blackwell BF, Dowding KJ, Cochran RJ, Dobranich D. Utilization of sensitivity coefficients to guide the design of a thermal battery. *Proceedings of the 1998 ASME/IMECE*. ASME: Anaheim, CA, 1998; 73–82, HTD-Vol. 561-5.
21. Turgeon É, Borggaard J, Pelletier D. A continuous sensitivity equation approach to optimal design in mixed convection. *Numerical Heat Transfer*, *Part A* 2000; **38**:869–885.
22. Turgeon É, Pelletier D, Borggaard J. Applications of continuous sensitivity equations to flows with temperature-dependent properties. *Numerical Heat Transfer*, *Part A*: *Applications* 2003; **44**:611–624.
23. Turgeon É, Pelletier D, Borggaard J. A general continuous sensitivity equation formulation for the k–ε model of turbulence. *International Journal of Computational Fluid Dynamics* 2004; **18**:29–46.
24. Ilinca F, Hétu J-F, Pelletier D. Three-dimensional simulation and design sensitivity analysis of the injection molding process. *International Polymer Processing* 2005; **20**:86–92.

25. Hristova H, Étienne S, Pelletier D, Borggaard J. A continuous sensitivity equation method for time-dependent incompressible laminar flows. *International Journal for Numerical Methods in Fluids* 2006; **50**:817–844.
26. Ilinca F, Pelletier D, Borggaard J. A continuous second-order sensitivity equation method for time-dependent incompressible laminar flows. *International Journal for Numerical Methods in Fluids* 2007; **55**:565–587.
27. Ilinca F, Pelletier D. A continuous shape sensitivity equation method for unsteady laminar flows. *ECCOMAS CFD 2006*, *European Congress on Computational Fluid Dynamics*, Egmond aan Zee, The Netherlands, September 2006.
28. Roache PJ. *Verification and Validation in Computational Science and Engineering*. Hermosa Publishers: Albuquerque, NM, 1998.
29. Sohankar A, Norberg C, Davidson L. Low-Reynolds-number flow around a square cylinder at incidence: study of blockage, onset of vortex shedding and outlet boundary condition. *International Journal for Numerical Methods in Fluids* 1998; **26**:39–56.
30. Williamson CHK. Defining a universal and continuous Strouhal–Reynolds number relationship for the laminar vortex shedding of a circular cylinder. *Physics of Fluids* 1988; **31**:2742–2744.
31. Behr M, Hastreiter S, Mittal S, Tezduyar TE. Incompressible flow past a circular cylinder: dependence of the computed field on the location of the lateral boundaries. *Computer Methods in Applied Mechanics and Engineering* 1995; **123**:309–316.

DOI: 10.1002/fld